J. Fluid Mech. (1972), *vol.* 53, *part* 2, *pp.* 305–327
Printed in Great Britain

Thermal instabilities in two-fluid horizontal layers

By RICHARD W. ZEREN
Department of Mechanical Engineering, Michigan State University
AND WILLIAM C. REYNOLDS
Department of Mechanical Engineering, Stanford University

(Received 4 January 1971 and in revised form 4 November 1971)

An analytical and experimental study of thermally induced instability in horizontal two-fluid layers is reported. A linear stability analysis for two initially motionless, viscous immiscible fluids confined between horizontal isothermal solid surfaces and subject to both density (Bénard) and surface-tension-gradient (Marangoni) driving mechanisms is presented. Calculations for the laboratory configuration reported below predict instability for heating from above or below. Response is strongly dependent on the ratios of the properties of the fluids, the total depth of the layer and the depth fraction of one fluid. Three different response modes occur (interfacial-tension-gradient dominated, buoyancy dominated and surface-deflexion dominated) depending on the fluid depth fractions. When the heating is from above, the buoyancy mechanism is stabilizing for most wavenumbers, including the critical one. Heating from below lowers the critical Marangoni number and adds a buoyancy driven response mode. Results of experimental measurements of the critical Marangoni number for layers of total depth 2 mm consisting of benzene over water with a water depth fraction of 0·40 are also presented. No instability was detected in any case for heating from above, even though the Marangoni number exceeds the predicted critical value by as much as five times. The critical Rayleigh number observed for heating from below falls between the critical values predicted with and without the Marangoni effect. The presence of surface contamination is believed to be responsible for the apparent lack of convection when heating is from above and for the difference between the predicted and measured critical Rayleigh number when heating is from below.

1. Introduction

Bénard's (1900) experimental study of the regular-hexagon circulation pattern in a thin layer of fluid heated from below has been the catalyst for many research papers. The onset of this 'cellular' motion in an initially stationary fluid has been of particular interest.†

Two principal cellular convection mechanisms have been identified: (i)

† An excellent review of cellular convection is presented by Berg, Acrivos & Boudart (1966).

buoyancy resulting from thermally induced density gradients (Bénard convection) and (ii) interfacial forces due to surface tension variations produced by temperature or concentration gradients (Marangoni convection). Associated with each of these mechanisms is a critical value of a parameter which divides stable from unstable initial states. An appropriate parameter for density gradient instability is the Rayleigh number

$$Ra = g\beta\Delta T d^3/\nu\kappa.$$

Here g is the acceleration due to gravity, $\beta = -\rho^{-1}(\partial\rho/\partial T)_p$ is the isobaric compressibility, ρ the density, p the pressure, ΔT the positive temperature difference across the layer, d the layer thickness, ν the kinematic viscosity and κ the thermal diffusivity. Surface-tension-gradient driven motion is often called the Marangoni effect; the relevant critical parameter is the Marangoni number

$$Ma = (-d\sigma/dT)\Delta T d/\mu\kappa.$$

Here, σ is the surface tension and μ the dynamic viscosity. Note that $d\sigma/dT$ is usually negative. The principal concern of theoretical analysis is the determination of critical Rayleigh or Marangoni number for a variety of initial states.

Bénard instability was first analysed by Rayleigh (1916). Subsequently Jeffreys (1926, 1928), Low (1929) and Pellew & Southwell (1940) extended and polished Rayleigh's work. Schmidt & Milverton (1935) and Silveston (1958) verified experimentally the predictions of the onset of Bénard convection in fluids confined between horizontal isothermal solid surfaces.

Pearson (1958) showed that the Marangoni effect can also cause an instability in a thin fluid layer. He considered a thin film of infinite extent with a solid bottom surface and free top surface. The surface tension was assumed to be a linear decreasing function of temperature and the deficit of surface tension force between two points on the interface was balanced by shear forces. He ignored gravity, and therefore density-gradient effects, and the effects of a superposed fluid. In addition the interface was assumed to remain flat (undeformed) and the heat-transfer coefficient on the upper surface was assumed to be independent of the convective motion. His analysis indicates instability only for heating from the solid boundary. For fluids where the surface tension increases with increasing temperature, instability occurs only for heating from the free surface.

Sternling & Scriven (1959) considered Marangoni instability induced by concentration gradients at the interface of two fluids. Buoyancy effects and surface deflexions were ignored. This model shows instability for mass transfer in either direction. They subsequently accounted for the effect of mean surface tension by allowing the surface to deflect (Scriven & Sternling 1964). Smith (1966) included gravity waves (but not buoyancy) in a two-fluid model and also found instability for heating in either direction. Nield (1964) applied Pearson's variable-surface-tension boundary condition to a fluid layer subject to buoyancy. He showed that when the mechanisms reinforce one another they are closely coupled. They also mutually influence the stability limit.

Despite the wide range of phenomena incorporated in previous analyses, no single one includes all the effects which would be present in an experiment subject

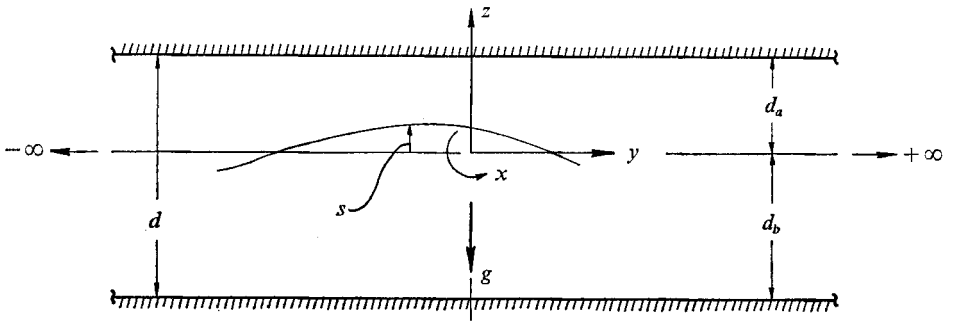

FIGURE 1. Co-ordinate frame for system model.

to Marangoni instability. Therefore a new analysis is necessary to support an experimental determination of critical Marangoni number. The model must include (i) two fluids to allow for instability for transfer in either direction, (ii) both the Bénard and the Marangoni effect (buoyancy should have a significant influence on stability limits), (iii) a deformable interface to account for the effect of mean surface tension, (iv) continuous temperature and heat flux across the interface. Such an analysis and corresponding experiments are presented in this paper. Calculated results for a particular case are compared with experimental data. This work is described in more detail in Zeren & Reynolds (1970), hereafter referred to as I.

2. Analysis

Consider two immiscible viscous fluids bounded by horizontal, isothermal solid surfaces of infinite extent, as shown in figure 1. A Cartesian co-ordinate system is established with g, the gravitational acceleration, in the negative z direction with z measured from the undisturbed interface. The upper fluid is designated as a (above) and the lower fluid as b (below), and the fluid depths are d_a and d_b, respectively. The total depth is d. Surface deflexions from the $z = 0$ plane are represented by $s(x, y, t)$, where t is time. In the initial state, the temperature, and thus the density, varies linearly in the z direction in each phase and the surface tension is uniform on the interface. When motion occurs the density of fluid particles may change and the interfacial tension may vary along the interface, but all other properties are presumed to be both uniform in each phase and constant in time.

The linearized dynamical equations describing departures from this initial state are well-known† (see Pellew & Southwell 1940, for example). They are, within each fluid, the continuity equation

$$\frac{\partial u}{\partial x}+\frac{\partial v}{\partial y}+\frac{\partial w}{\partial z} = 0, \tag{1}$$

† For a detailed derivation of these equations including a discussion of the applicability of the Boussinesq approximation for variable density fluids see I.

momentum equation

$$\frac{\partial}{\partial t}\begin{pmatrix}u\\v\\w\end{pmatrix} = -\frac{1}{\rho}\begin{pmatrix}\partial/\partial x\\\partial/\partial y\\\partial/\partial z\end{pmatrix}p + \begin{pmatrix}0\\0\\\beta g\theta\end{pmatrix} + \nu\nabla^2\begin{pmatrix}u\\v\\w\end{pmatrix} \tag{2}$$

and energy equation $$\partial\theta/\partial t + \gamma w = \kappa\nabla^2\theta. \tag{3}$$

Here u, v, w are the x, y, z components of the disturbance velocity, respectively, p is the disturbance pressure, θ the disturbance temperature, γ the initial temperature gradient and $\nabla^2 = \partial^2/\partial x^2 + \partial^2/\partial y^2 + \partial^2/\partial z^2$.

The velocity and temperature perturbations must vanish on the solid surfaces, requiring

$$\left.\begin{aligned} u_a = v_a = w_a = \theta_a = 0 \quad &\text{on} \quad z = d_a, \\ u_b = v_b = w_b = \theta_b = 0 \quad &\text{on} \quad z = -d_b. \end{aligned}\right\} \tag{4}$$

The interface conditions are transferred from $z = s(x, y, t)$ to $z = 0$ by Taylor expansion. The resulting linearized interfacial conditions (to be applied at $z = 0$) are as follows.

Kinematic condition (for each fluid):

$$w = \partial s/\partial t. \tag{5}$$

Continuity of velocity, temperature and heat flux:

$$u_a = u_b, \quad v_a = v_b, \quad w_a = w_b, \tag{6}$$

$$\theta_a + \gamma_a s = \theta_b + \gamma_b s, \tag{7}$$

$$k_a\frac{\partial\theta_a}{\partial z} = k_b\frac{\partial\theta_b}{\partial z}, \tag{8}$$

where k is the thermal conductivity.

Lateral stress continuity:

$$\mu_a\left(\frac{\partial w_a}{\partial x} + \frac{\partial u_a}{\partial z}\right) - \mu_b\left(\frac{\partial w_b}{\partial x} + \frac{\partial u_b}{\partial z}\right) = -\frac{d\sigma}{dT}\left(\frac{\partial\theta_b}{\partial x} + \gamma_b\frac{\partial s}{\partial x}\right), \tag{9}$$

$$\mu_a\left(\frac{\partial w_a}{\partial y} + \frac{\partial v_a}{\partial z}\right) - \mu_b\left(\frac{\partial w_b}{\partial y} + \frac{\partial v_b}{\partial z}\right) = -\frac{d\sigma}{dT}\left(\frac{\partial\theta_b}{\partial y} + \gamma_b\frac{\partial s}{\partial y}\right). \tag{10}$$

Vertical stress continuity:

$$p_b - p_a + (\rho_a - \rho_b)gs - 2\mu_b\frac{\partial w_b}{\partial z} + 2\mu_a\frac{\partial w_a}{\partial z} + \sigma\left(\frac{\partial^2 s}{\partial x^2} + \frac{\partial^2 s}{\partial y^2}\right) = 0. \tag{11}$$

All fluid properties are evaluated at the initial interface temperature.

The dynamical equations and the boundary equations are linear and homogeneous in the disturbance variables u, v, w, p, θ and s. Hence they define an eigenvalue problem in which the eigenfunctions correspond to the particular disturbances for which the convective motion can begin. Since the coefficients

are independent of time, the eigenfunctions are assumed to have the form

$$\begin{pmatrix} u \\ v \\ w \\ p \\ \theta \\ s \end{pmatrix} = \begin{pmatrix} \hat{u}(z)\,\tilde{U}(x,y) \\ \hat{v}(z)\,\tilde{V}(x,y) \\ \hat{w}(z)\,\tilde{W}(x,y) \\ \hat{p}(z)\,\tilde{P}(x,y) \\ \hat{\theta}(z)\,\tilde{\Theta}(x,y) \\ \hat{s} \quad \tilde{S}(x,y) \end{pmatrix} e^{qt} + \text{complex conjugate}, \tag{12}$$

where both the z and the (x, y) functions and $q = q_r + iq_i$ are in general complex. The complex conjugate is necessary to yield the necessarily real solutions for the physical problem.

The parameter q is the eigenvalue associated with a particular disturbance. If $q_r > 0$, the associated disturbance grows and the initial state is unstable to that disturbance; if $q_r < 0$, the disturbance decays and the initial state is stable. Disturbances for which $q_r = 0$ are neither amplified nor damped and therefore are called marginally stable. For a marginally stable disturbance q_i need not be zero; fixed amplitude periodic disturbances may exist. If for all marginally stable and amplified disturbances q_i is always zero (no oscillatory motions) the equations can be greatly simplified by setting $q \equiv 0$. This circumstance is commonly called the 'exchange of stabilities'. Exchange of stabilities has been proved valid for density-gradient convection subject to a variety of boundary conditions (Pellew & Southwell 1940) and for surface-tension-gradient convection in one fluid subject to Pearson's surface condition (Vidal & Acrivos 1966). This exchange was assumed without proof by Pearson (1958), Scriven & Sternling (1964), Nield (1964) and Smith (1966). However, Sternling & Scriven (1959) found both stationary and oscillatory marginal states for a two-fluid Marangoni convection model. There is, therefore, some doubt about when the exchange of stabilities assumption is valid. If $q_i = 0$ is assumed and instability is found, the apparent critical Marangoni number must be an upper bound on the true critical Marangoni number. With due appreciation of this implication, the exchange of stabilities is assumed here and q is set identically zero. Some other parameter of the problem, such as the Rayleigh or Marangoni number, may now be used as the eigenvalue, with its value defining a state of marginal stability.

Substitution of (12) into (1), (2) and (3) and extraction of the equations describing $\hat{w}(z)$ and $\hat{\theta}(z)$ yields, in each fluid,

$$(D^2 - \alpha^2)^2\,\hat{w}(z) = (\alpha^2 \beta g/\nu)\,\hat{\theta}(z) \tag{13}$$

and

$$(D^2 - \alpha^2)\,\hat{\theta}(z) = (\gamma/\kappa)\,\hat{w}(z), \tag{14}$$

where $D = d/dz$ and α is the disturbance wavenumber. Eigensolutions in the form (12) are found to exist only for disturbances which satisfy

$$(\nabla_{\mathrm{II}}^2 + \alpha^2)\,\tilde{W}(x,y) = 0. \tag{15}$$

where $\nabla_{\mathrm{II}}^2 = \partial^2/\partial x^2 + \partial^2/\partial y^2$, and only when $\tilde{W}(x,y) = \tilde{\Theta}(x,y) = \tilde{S}(x,y) = \tilde{P}(x,y)$,

n	1, 2	3,4	5,6	
ω_n	1	$e^{\frac{2}{3}i\pi}$	$e^{-\frac{2}{3}i\pi}$	if $g\gamma\beta > 0$
	-1	$e^{\frac{1}{3}i\pi}$	$e^{-\frac{1}{3}i\pi}$	if $g\gamma\beta < 0$

TABLE 1

$\tilde{U}(x,y) = \partial\tilde{W}/\partial x$ and $\tilde{V}(x,y) = \partial\tilde{W}/\partial y$. Also, the vertical boundaries must be impermeable surfaces of symmetry, which corresponds to an array of cells in a fluid of infinite extent. Solutions to (15) for all close-packing plan-form geometries are known (Pellew & Southwell 1940). Equations (13) and (14) hold for any plan form.

The equations and boundary conditions are now combined to obtain a manageable set from which the eigenfunctions and eigenvalues are obtained. Substituting for $\hat{w}(z)$ from (14) into (13) gives within each fluid

$$\{(D^2-\alpha^2)^3-\alpha^2\beta g\gamma/\nu\kappa\}\hat{\theta}(z) = 0. \tag{16}$$

After elimination of u, v and p by manipulation of (1) and (2) the interface conditions (at $z = 0$) become

$$\hat{w}_a = \hat{w}_b = 0, \tag{17}$$

$$D\hat{w}_a = D\hat{w}_b, \tag{18}$$

$$\hat{\theta}_a+\gamma_a\hat{s} = \hat{\theta}_b+\gamma_b\hat{s}, \tag{19}$$

$$k^*D\hat{\theta}_a = D\hat{\theta}_b, \tag{20}$$

where $k^* = k_a/k_b$,

$$\mu^*(D^2-\alpha^2)\,\hat{w}_a-(D^2-\alpha^2)\,\hat{w}_b = (-d\sigma/dT)\,\alpha^2/\mu_b[\hat{\theta}_b+\gamma_b\hat{s}] \tag{21}$$

and

$$(D^2-3\alpha^2)\,D\hat{w}_b-\mu^*(D^2-3\alpha^2)\,D\hat{w}_a = \alpha^2/\mu_b[\rho_b-\rho_a+\alpha^2\sigma]\,\hat{s}, \tag{22}$$

where $\mu^* = \mu_a/\mu_b$ and (9) and (10) have collapsed into (21). At $z = d_a$

$$\hat{w}_a = 0, \quad D\hat{w}_a = 0, \quad \hat{\theta}_a = 0 \tag{23}$$

and at $z = -d_b$

$$\hat{w}_b = 0, \quad D\hat{w}_b = 0, \quad \hat{\theta}_b = 0. \tag{24}$$

Note that continuity of temperature in the initial state requires that $k^* = \gamma_b/\gamma_a$. The problem now consists of a sixth-order equation for $\hat{\theta}$ with each fluid (equation (16)), twelve boundary conditions and an equation for the surface deflexion $\hat{s}$.

The general solution to (16) is, in each fluid,

$$\hat{\theta}_\phi(z) = \sum_{n=1}^{6} C_{\phi,n}\,e^{r_{\phi,n}z}, \tag{25}$$

where the $C_{\phi,n}$ are as yet unknown constants and $\phi = a$ denotes the upper fluid and $\phi = b$ the lower. Here

$$r_{\phi,n} = (-1)^{n+1}\alpha(1+\omega_n\mathscr{R}_\phi)^{\frac{1}{2}},$$

where

$$\mathscr{R}_\phi = |(g\gamma\beta/\nu\kappa\alpha^4)^{\frac{1}{3}}|$$

and ω_n is as given in table 1, so that ω_5 and ω_6 are the complex conjugates of ω_3 and ω_4 respectively.

Substitution of (25) into the appropriate boundary and interface conditions, (17)–(24), yields thirteen linear homogeneous algebraic equations for the thirteen unknown constants $C_{\phi,n}$ and $\gamma_b \hat{s} = C_{13}$. For the solutions to be non-trivial, the characteristic determinant D of the coefficient matrix C must vanish. The coefficient matrix may be non-dimensionalized by referring all lengths to the total gap width d, by defining $d_a^* = d_a/d$, $d_b^* = d_b/d$, $\alpha^* = \alpha d$, $r_{\phi,n}^* = r_{\phi,n} d$ and then dividing each row by appropriate property groupings. For details see I.

The dimensionless groups arising out of this analysis are the following:

Rayleigh number $$Ra_b = g\beta_b \gamma_b d^4/\nu_b \kappa_b,$$

Marangoni number $$Ma_b = (-d\sigma/dT)\gamma_b d^2/\mu_b \kappa_b,$$

Bond number $$Bo_b = g\rho_b d^2/\sigma,$$

Crispation group $$Cr_b = \mu_b \kappa_b/\sigma d,$$

and the physical property ratios $\kappa^* = \kappa_a/\kappa_b$, k^*, μ^*, $\beta^* = \beta_a/\beta_b$ and $\rho^* = \rho_a/\rho_b$. Notice that no arbitrary scaling of the velocity is made. Also note that the Rayleigh and Marangoni numbers are negative for heating from below and positive for heating from above.

Either Ra_b or Ma_b can be considered as the eigenvalue, but for any given initial state $$Ra_b/Ma_b = \rho_b g\beta_b d^2/(-d\sigma/dT) = \Gamma,$$

a constant, i.e. independent of temperature. The characteristic determinant then explicitly depends on eleven parameters: Ma_b, Γ, Bo_b, Cr_b, d_b^*, κ^*, μ^*, k^*, ρ^*, β^* and α^*. The smallest value of Ma_b for which $D = 0$ is determined by varying Ma_b for a given parameter set and α^* until D vanishes. Since Ma_b is transcendentally imbedded in the elements of C, an iterative solution is necessary. Since the elements are also complex, the real and imaginary parts of D must vanish identically for a real value of Ma_b. However, a closer inspection of (16) and the boundary conditions reveals that no complex quantities appear. Since the operator is real, the complex conjugate operator must also be real, and the solutions represented in (25) are real. There is, therefore, a real representation of the matrix eigenvalue problem, and the zeros of D may be found by varying the real eigenvalue Ma_b.

If $k^* = 1$, $\rho^* = 1$ and $\sigma = 0$ the coefficients of $C_{13} = \gamma_b \hat{s}$ vanish identically, column 13 of C is filled with zeros and D is always zero. This circumstance occurs only if there is in fact only one fluid. The equations, boundary conditions and coupling conditions are still valid (with the appropriate terms equal to zero) and apply to the one-fluid buoyancy problem. However, since flow may now cross the 'interface', the vertical velocity component on the interface is not necessarily zero. By imposing this condition as row 13 of the coefficient matrix it is possible to reduce C to a 12×12 matrix and treat the one-fluid buoyancy problem. Since there is no interface for one fluid the loss of column 13 is acceptable. The coupling conditions are now applied on an artificial or 'phantom' interface.

A digital computer program was written to automatically find the zeros of D. A single program treats the coupled Marangoni–Bénard problem, the one-fluid buoyancy problem and the two-fluid buoyancy problem with $d\sigma/dT$ set identically zero. The program has been checked by computing the critical Rayleigh

numbers for the one-fluid Bénard problem by dropping row and column thirteen of C as discussed above. Results for various locations of the phantom interface (various values of d^*) agree quite well with the definitive eigenvalues reported by Reid & Harris (1958) (see I).

Once the eigenvalues are known, the constants $C_{\phi,n}$ and hence the eigenfunctions are found. As a check of the computing program, eigenfunctions for the one-fluid buoyancy problem were verified by comparison with the eigenfunctions calculated by Reid & Harris (1958).

Additional information about the interactions of the two driving mechanisms and the source of the driving energy was found from the integral mechanical energy equation for the perturbation flow. If the linearized disturbance momentum equations in each fluid are multiplied by the velocity components u_i, summed and integrated over the volume V_ϕ of one 'cell', the integral mechanical energy equation for the perturbation results:

$$\int_{V\phi} u_i \frac{\partial u_i}{\partial t} dV_\phi = -\frac{1}{\rho}\int_{V\phi} u_i \frac{\partial p}{\partial x_i} dV_\phi + \beta g \int_{V\phi} \theta w \, dV_\phi + \nu \int_{V\phi} u_i \frac{\partial \tau_{ij}}{\partial x_j} dV_\phi. \tag{26}$$

Here V_ϕ is the cell volume in each fluid and

$$\tau_{ij} = \partial u_i/\partial x_j + \partial u_j/\partial x_i.$$

Summation notation is used. The left-hand integral is the time rate of change of the kinetic energy of the perturbation. This term is zero for the marginal case with the exchange of stabilities assumed. The first term on the right is the interaction of the pressure and velocity fields, the second is the energy input due to the buoyancy driving mechanism and the third term is the shear work term.

These terms can be evaluated for disturbances of the form of (12). The x, y dependence then is confined to the positive-definite integral $I^2 = \int_A \hat{W}^2 dA$, where A is the cell cross-sectional area, which is the same for each fluid. Evaluation of the buoyancy integral is straightforward. With the help of Green's identities the pressure-velocity integral can be shown to be zero everywhere except on the interface. The pressure then may be eliminated and the integral written in terms of $\hat{w}(0)$ and I^2. The shear work term contains the work input to the fluid at the surface and the dissipation integral. Applying Green's identity to this integral gives

$$\nu \int_{V\phi} u_i \frac{\partial \tau_{ij}}{\partial x_j} dV_\phi = -\nu \int_{V\phi} \tau_{ij} \frac{\partial u_i}{\partial x_j} dV_\phi + \nu \int_S u_i \tau_{ij} \cos(n, x_j)\, dS, \tag{27}$$

where n is measured along the outward-pointing normal to the cell surface S and $\cos(n, x_j)$ is the cosine of the angle between n and x_j.

The surface integral, which is now in the form of a power input, vanishes on the solid wall because $u_i \equiv 0$ and on the vertical cell walls because the walls are shear-free impermeable and parallel to z. The integral $\mp \nu \int_{S_I} u_i \tau_{i3} dS_I$ over the interface S_I remains, where the signs reflect the alignment of z with n so that the upper sign goes with the upper fluid and the lower sign with the lower fluid. The disturbance (12) is substituted and u and v eliminated to give

$$\mp \nu \alpha^{-2} D\hat{w}(0)\,[D^2\hat{w}(0) + 3\alpha^2 \hat{w}(0)]\, e^{2qt} I^2. \tag{28}$$

The volume integral on the right of equation (27) is commonly called the dissipation integral. Substituting (12) and eliminating u and v yields

$$-\nu e^{2qt}\left\{2\alpha^{-2}\int_z (D\hat{w})^2\,dz\int_A\left[\left(\frac{\partial^2\tilde{W}}{\partial x^2}\right)^2+2\left(\frac{\partial^2\tilde{W}}{\partial x\,\partial y}\right)^2+\left(\frac{\partial^2\tilde{W}}{\partial y^2}\right)^2\right]dA\right.$$
$$\left.+2I^2\int_z (D\hat{w})^2\,dz+I^2\int_z (D^2\hat{w}+\alpha^2\hat{w})^2\,dz\right\}. \quad (29)$$

The area integral in (29) may be shown to equal $\alpha^4 I^2$ by using Green's identity for a surface integral and equation (15).

For the case of marginal stability, then, the disturbance mechanical energy equation may be written as

$$\frac{dE_\phi}{dt}=0=\pm\nu\alpha^{-2}\hat{w}(0)\,[D^2-\alpha^2]\,D\hat{w}(0)+\beta g\int_z\hat{\theta}\hat{w}\,dz$$
$$-\nu\left\{\int_z\{4(D\hat{w})^2+\alpha^{-2}[(D^2+\alpha^2)\hat{w}]^2\}\,dz\pm\alpha^{-2}D\hat{w}(0)\,[D^2+3\alpha^2]\,\hat{w}(0)\right\}. \quad (30)$$

Here E_ϕ is the kinetic energy in each phase divided by I^2 and the integration limit z indicates integration over z in the direction appropriate to the cell and phase being considered. This development is presented in more detail in I.

The first term on the right-hand side is the power input to the fluid from the pressure on the interface; where $q=0$ and a distinct interface exists this term is zero since $\hat{w}(0)$ is zero. For the one-fluid buoyancy problem, where $w(0)\neq 0$, energy may be transferred across the phantom interface owing to pressure forces but the net increase or decrease of total energy is zero. The next term is the power input from the buoyancy forces. For a stably stratified density this term should always be negative since work must be done to upset the stable equilibrium. The term in curly brackets contains the viscous dissipation integral and the surface-shear work term. The dissipation is always negative. The net surface power contribution is the measure of power input from the Marangoni effect. If the Marangoni effect is present, the variation in surface tension may or may not be doing work on the fluid, depending on the velocity and temperature at the interface. If the Marangoni effect has been suppressed, the surface term can only be zero.

Comparison of the net power inputs from the buoyancy and surface tension mechanisms indicates the principal energy source driving the instability.

3. Numerical calculations

3.1. *Specific calculated system*

Calculations were made for layers of benzene over water with a total depth of 2 mm and various water depth fractions d_b^*. Experiments for this configuration are reported in §4. Water and benzene were selected because they meet the criterion established by Sternling & Scriven (1959) for instability for heating from either direction; both the kinematic viscosity and thermal diffusivity of water are greater than those of benzene. This criterion is met for few combinations of immiscible liquids. Liquids also preclude radiant heat exchange at the

T	k^*	κ^*	ρ^*	μ^*	β^*	Γ	Bo_b^{-1}	Bo_b/Cr_b
16 °C	0·274	0·730	0·886	0·605	7·06	0·142	0·840	548000
36 °C	0·240	0·600	0·872	0·766	3·00	0·256	0·825	807000

TABLE 2. Summary of property ratios and parameters

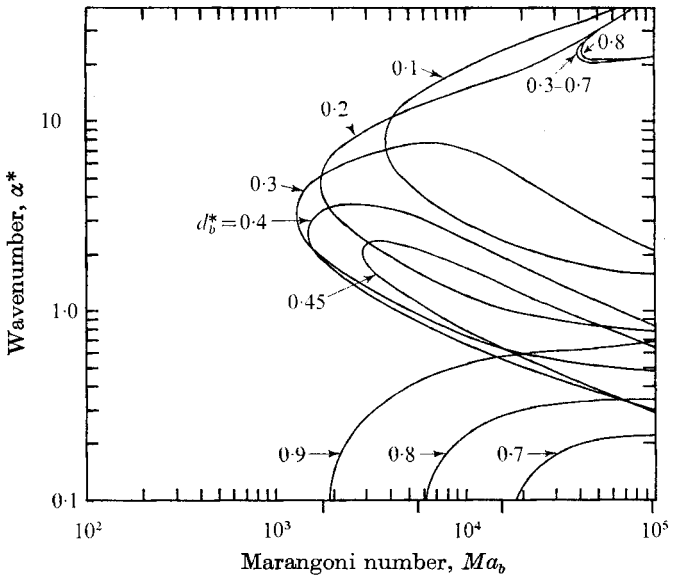

FIGURE 2. Marginally stable Marangoni number as a function of wavenumber for various water depth fractions for heating from above. Benzene over water, total depth = 2 mm.

interface, which agrees with the model, and make the temperature differences across each layer more nearly equal than if a gas and a liquid are used. Water and benzene are also readily available in chemically pure (reagent) grades and their properties are well-known, so that they can be used for experiments. Properties and property ratios evaluated at two temperatures bounding the experiments described below are summarized in table 2. Most calculations were made for properties at 16 °C.

The (α–Ma_b) plane was searched for the zeros of D corresponding to the smallest Marangoni numbers. The results are compared with the equivalent pure Marangoni effect case as calculated by Smith (1966). Representative eigenfunctions and energy integrals are also presented. An asymptotic analysis for $\alpha^* \to 0$ prompted by these results is described in the appendix. For more detail see I.

3.2. *Results for heating from above*

The Marangoni number as a function of wavenumber for heating from above is shown in figure 2. Critical Marangoni numbers and corresponding wavenumbers are tabulated in table 3. Since the initial temperature gradient is positive for heating from above, the Marangoni number is positive.

The system appears to respond in three different modes depending on the

	Heating from above			Heating from below				
				Marangoni number			Rayleigh number	
d_b^*	α_{CR}^*	Marangoni number $\frac{(-d\sigma/dT)\gamma_b d^2}{\mu_b \kappa_b}$	α_{CR}^*	$\frac{(-d\sigma/dT)\gamma_b d^2}{\mu_b \kappa_b}$	$\frac{(-d\sigma/dT)\gamma_a d_a^2}{\mu_a \kappa_a}$ benzene	$\frac{(-d\sigma/dT)\gamma_b d_b^2}{\mu_b \kappa_b}$ water	$\frac{g\beta_a \gamma_a d_a^4}{\mu_a \kappa_a}$ benzene	$\frac{g\beta_b \gamma_b d_b^4}{\mu_b \kappa_b}$ water
0·1	8	3747	3·5	−371	−2473	−3·7	−1780	−0·005
0·2	5	1701	4·2	−780	−4108	−31·2	−2336	−0·18
0·3	3·3	1266	5·8	−1976	−7968	−178	−3468	−2·3
0·4	2·6	1486	9	−6068	−17980	−971	−5749	−22
0·45	2·1	2880	—	—	—	—	—	—
0·5	22	39600	12	−15070	−31000	−3770	−6880	−134
0·6	22	39500	2·5	−1950	−2570	−703	−366	−36·0
0·7	0	15260	2·8	−728	−539	−357	−43·1	−24·8
0·8	0	5478	3	−615	−202	−394	−7·2	−35·8
0·9	0	1734	3·2	−963	−79·3	−0·780	−0·7	−89·7

TABLE 3. Critical Rayleigh and Marangoni numbers for layers of benzene over water with 2 mm total depth

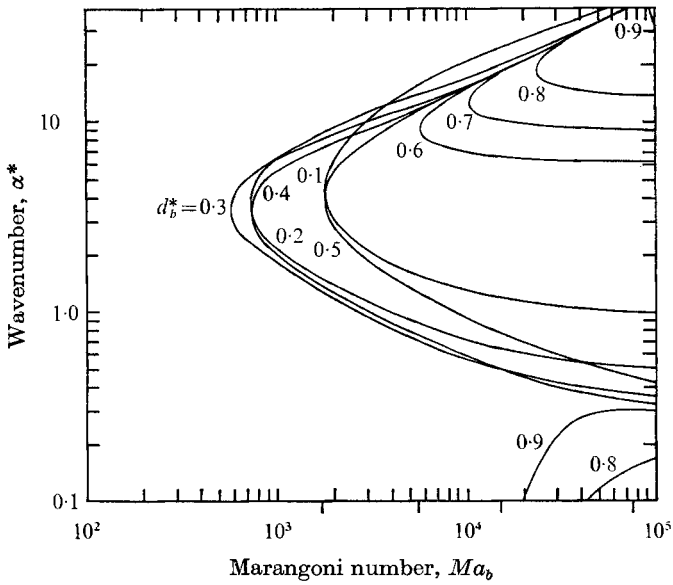

FIGURE 3. Marginally stable Marangoni number as a function of wavenumber and depth fraction for pure Marangoni effect flow as calculated from Smith (1966). Heating from above. Benzene over water, total depth = 2 mm.

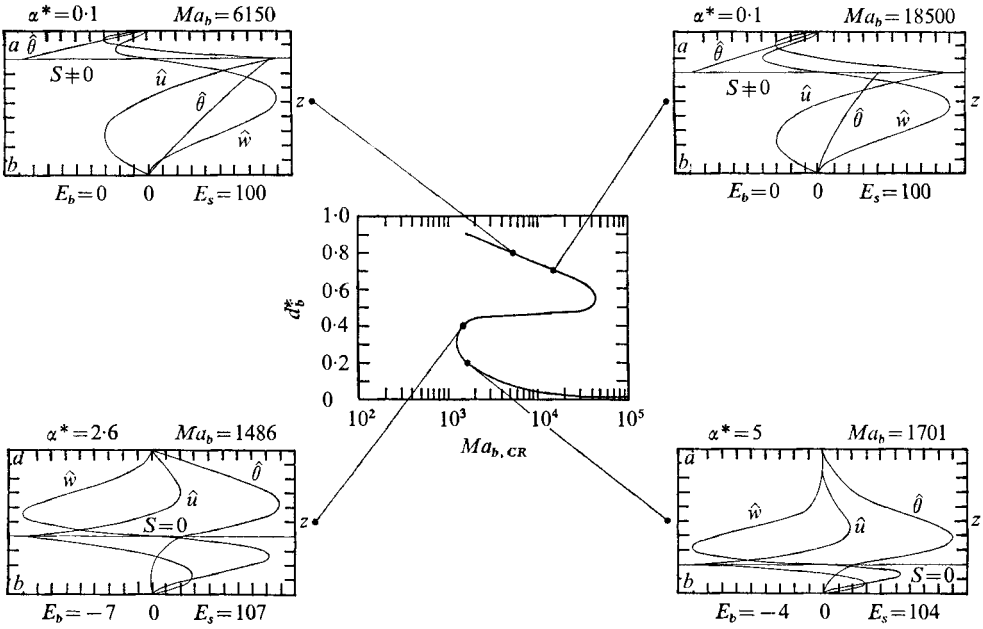

FIGURE 4. Variation of critical Marangoni number, eigenfunctions and energy integrals with depth fraction for heating from above. Benzene over water, total depth = 2 mm. E_b = buoyancy energy integral, E_s = surface work term, as percentage of dissipation integral, S = surface deflexion.

water depth fraction d_b^*. As the depth fraction increases from 0·1, the system is most unstable to disturbances of moderate wavenumber, corresponding to disturbance scales of the order of the total depth. As d_b^* increases to about 0·4 the configuration becomes stable for all but a narrow wavenumber range. For d_b^* exceeding about 0·48, the minimum Marangoni number for moderate wavenumber is greater than 10^5, and the least stable state then corresponds to large wavenumber, or small-scale, disturbances. As d_b^* increases beyond about 0·65 the critical Marangoni is associated with $\alpha^* = 0$, an infinitely large-scale disturbance. Asymptotic values of critical Marangoni number for $\alpha^* \to 0$ (see appendix) are shown as tick marks below the $\alpha^* = 0{\cdot}1$ axis. The variation of the critical Marangoni number with depth fraction is shown in figure 4.

Critical Marangoni numbers calculated from Smith's (1966) analysis for purely surface-tension driven flow are shown in figure 3. Comparison of figures 2 and 3 shows that addition of the stable density gradient increases the critical Marangoni number for the moderate and large wavenumber disturbances, as would be expected. The critical wavenumber is also shifted, as are the asymptotes of the curves for $Ma_b \to \infty$. The filtering effect of the density gradient suggested in figure 2 is confirmed; disturbances corresponding to moderate wavenumbers which are unstable for the pure Marangoni effect case are stabilized by the density gradient. The critical Marangoni number for $\alpha^* \to 0$ is again shown by tick marks below the axis. Apparently there is very little density influence on the value of the critical Marangoni number at $\alpha^* = 0$.

Eigenfunctions $\hat{w}(z)$, $\hat{\theta}(z)$ and $\hat{u}(z)$ at the critical states (except for the low wavenumber cases where they are calculated for $\alpha^* = 0{\cdot}1$) and the energy integral terms are shown in figure 4. Each of these eigenfunctions has been scaled to fill the diagrams. Actual flow patterns also depend on $\tilde{W}(x, y)$, $\tilde{\Theta}(x, y)$ and $\tilde{U}(x, y)$. The temperature and vertical velocity component have the same x, y dependence and their relative signs and shapes are properly shown in the figure. However, since $U = \partial \tilde{W}/\partial x$ and the sign of the derivative is not known, $\hat{u}$ may not be shown correctly related to $\hat{w}$ and $\hat{\theta}$. Selection of a cell cross-sectional shape and thus an x, y dependence is necessary to determine the proper relations. The total buoyancy integral E_b and surface power term E_s are given as percentages of the total dissipation integral, usually rounded off to the nearest whole number. The surface deflexion is indicated by S. For cases where surface deflexion occurs, $S \neq 0$, the perturbation temperature eigenfunctions $\hat{\theta}_a$ and $\hat{\theta}_b$ are not continuous across $z = 0$, as shown by (19). The temperature is continuous across the interface, however.

The eigenfunction curves show surface deflexions for small wavenumber critical states while no surface deflexions occur for moderate wavenumber critical states. The small wavenumber large-scale disturbances might be thought of as a tipping of the surface. The temperature eigenfunctions for these disturbances are nearly linear, indicating a minimum response to a surface motion. As shown by the energy terms, there is very little energy drain from the surface power input to the stirring of the stable density stratification for these disturbances. This helps to explain the slight differences between critical Marangoni numbers with and without the density gradient. On the other hand, there is a noticeable energy

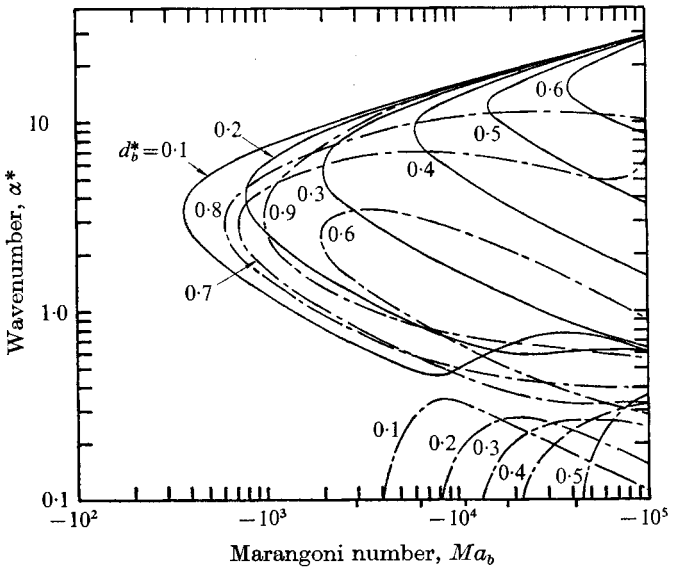

FIGURE 5. Marginally stable Marangoni number as a function of wavenumber for various water depth fractions for heating from below. Benzene over water, total depth = 2 mm. ——, buoyancy mode; — · —, surface deflexion mode for $d_b^* = 0{\cdot}1$–$0{\cdot}5$, Marangoni effect mode for $d_b^* = 0{\cdot}6$–$0{\cdot}9$.

drain to the buoyancy field for the critical states corresponding to moderate wavenumbers and this increases as d_b^* increases. Comparison of the eigenfunctions for $d_b^* = 0{\cdot}2$ and $0{\cdot}4$ shows that more fluid is involved in the motion for $d_b^* = 0{\cdot}4$ and thus a greater energy is necessary to upset the stable density gradient. The critical Marangoni number for $d_b^* = 0{\cdot}4$ is lower because of the reduced temperature drop across the shallower benzene layer.

The sensitivity of the moderate wavenumber disturbances to depth fraction around $d_b^* = 0{\cdot}5$ is presumably due to the increased energy demand indicated in figure 4. The surface mechanism is unable to supply sufficient energy to drive these larger scale motions against the stabilizing density gradient and the small-scale larger wavenumber motions are excited. Because of numerical difficulties, eigenfunctions and energy integrals could not be calculated for the large wavenumber cases. It is hypothesized that these disturbances are confined near the interface and require less energy to excite than the moderate wavenumber disturbances. The critical temperature difference for these cases is about 100 °C and they are therefore of little practical interest.

3.3. *Results for heating from below*

The Marangoni number for heating from below is shown as a function of wavenumber in figure 5. Critical Marangoni numbers and corresponding wavenumbers are tabulated in table 3. The Marangoni number is negative for heating from below because the initial temperature gradient is negative.

Again there seem to be three response modes. A regular pattern of stability curves for d_b^* increasing from $0{\cdot}1$ and for moderate wavenumbers is shown with

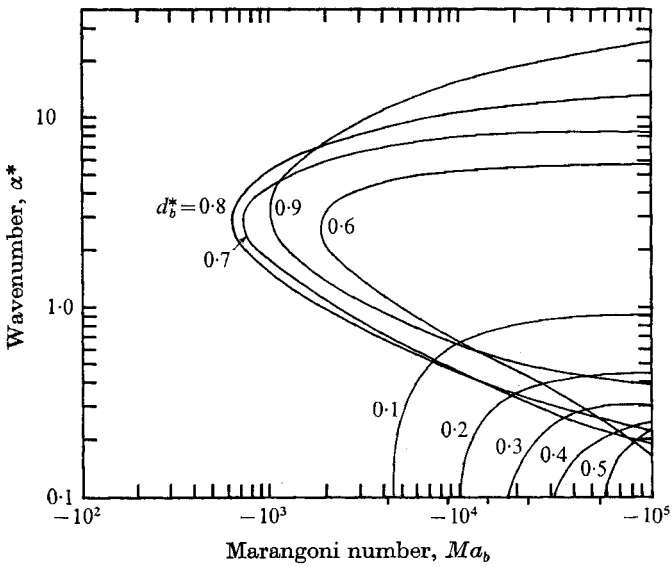

FIGURE 6. Marginally stable Marangoni number as a function of wavenumber and depth fraction for pure Marangoni effect flow as calculated from Smith (1966). Heating from below. Benzene over water, total depth = 2 m.

solid lines. In the same depth fraction range a second mode has a minimum Marangoni number at $\alpha^* = 0$ which is always greater than the minimum Marangoni number for the first mode. A third mode occurs for d_b^* greater than about 0·6, with the minimum Marangoni number corresponding to moderate wavenumber. The variation of the critical Marangoni number with depth fraction is shown in figure 7.

Comparison can be made with results based on Smith's (1966) pure Marangoni effect model, figure 6. The most striking difference is that the first mode (solid line in figure 5) does not appear for purely surface-tension driven motion, suggesting a buoyancy initiated instability. The second and third modes apparently correspond to Marangoni convection. The minimum Marangoni numbers are only slightly displaced for these modes. In fact the stability curves for $d_b^* = 0{\cdot}7$, 0·8, and 0·9 with and without the buoyancy effect fall on top of one another except at wavenumbers greater than about three times the critical wavenumber. The lowering of the critical Marangoni number for small wavenumber disturbances at small d_b^* apparently results from the additional driving mechanism.

The eigenfunctions and energy integrals in figure 7 tend to confirm the conclusions made above. The energy input to the perturbation field for the critical state corresponding to $d_b^* = 0{\cdot}8$ comes almost entirely from the surface work terms. For $d_b^* = 0{\cdot}2$ and 0·5, the buoyancy term makes a significant contribution to the energy input. The small wavenumber mode, which again involves an interface deflexion, is driven primarily by the Marangoni effect with a small contribution from the buoyancy field.

Critical Rayleigh and Marangoni numbers for heating from below and based on the properties, temperature gradients and depths of each phase are shown in

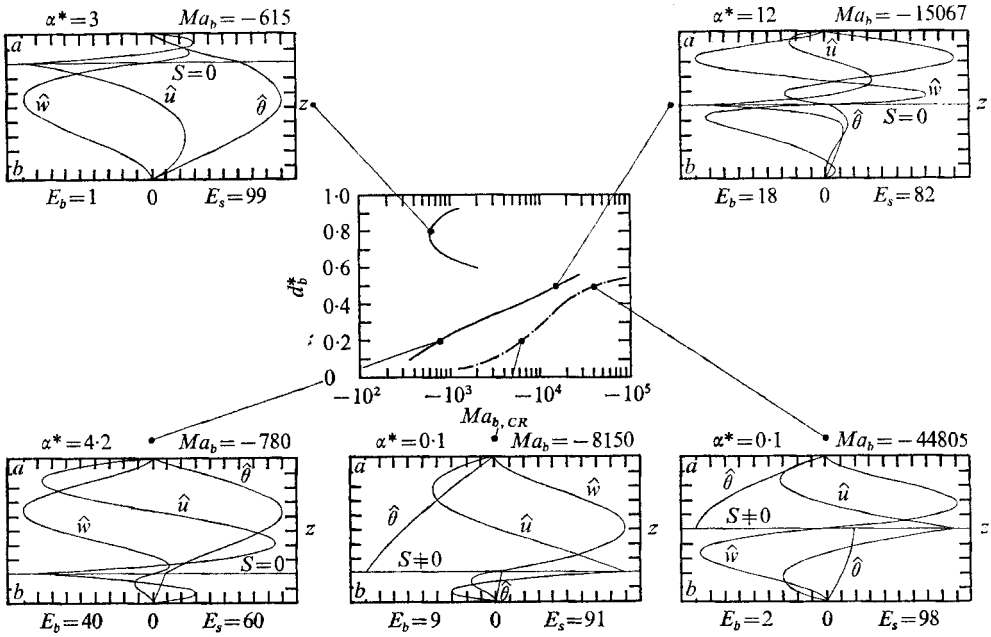

FIGURE 7. Variation of critical Marangoni number, eigenfunctions and energy integrals with depth fraction for heating from below. Benzene over water, total depth = 2 mm. E_b = buoyancy energy integral, E_s = surface work term as percentage of dissipation integral, S = surface deflexion.

table 3. The Rayleigh numbers for the water phase remain substantially below 669, the critical value for fluid resting on an isothermal solid surface with a constant heat flux free upper surface (Nield 1964). This implies that the water is essentially passive to buoyancy driven motions. The benzene is also apparently passive to the buoyancy mechanism when $d_b^* = 0{\cdot}6, 0{\cdot}7, 0{\cdot}8$ and $0{\cdot}9$ (but not otherwise), which strengthens the conclusion that the instability is driven by the Marangoni effect.

The benzene-phase Rayleigh number for the buoyancy driven modes ($d_b^* = 0{\cdot}1$ to $0{\cdot}5$) exceeds 1708, the critical Rayleigh number for a single fluid confined between horizontal isothermal surfaces, and the expected upper stability limit for a single fluid. This suggests that the buoyancy instability is driven from the benzene phase and that the Marangoni effect tends to retard the onset of motion.

Examination of the eigenfunctions for the buoyancy mode critical states tends to substantiate the passive role of the water phase. The water perturbation temperature profiles are nearly linear, giving the minimum response necessary to maintain temperature and heat flux continuity at the interface. The velocity component response also appears to be minimal. The eigenfunctions for the Marangoni effect mode show much more involvement of the water in the motion.

The retarding action of the Marangoni effect is also supported by study of the eigenfunctions. The eigenfunctions for the critical states of the buoyancy driven mode all show a zero in $\hat{w}(z)$ in the benzene phase. Thus *two* vertical cells occur in the benzene phase, one near the surface, associated with the Marangoni effect, and

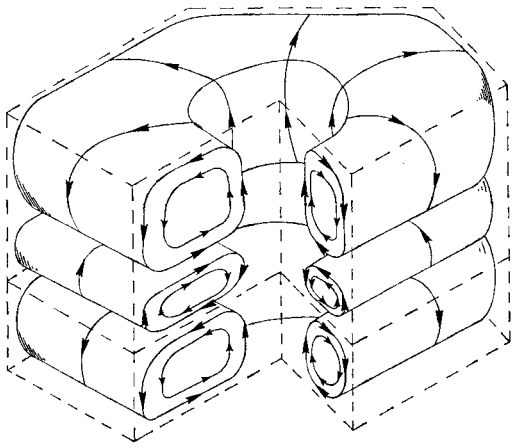

FIGURE 8. Convection cell for the buoyancy mode instability showing two cells in the benzene phase.

one in the bulk of the fluid, associated with buoyancy. The horizontal velocity components have three zeros in the benzene phase. A reversal of these components occurs near the top of the surface cell, indicating that the surface tension gradient causes flow opposite to the pattern which would result from the buoyancy mechanism alone. A sketch of this response appears in figure 8.

The velocity patterns also can be inferred from direct consideration of the driving mechanisms. The water heated from below is unstably stratified but the Rayleigh number is always far too small for self-sustaining buoyancy convection to occur. The benzene, therefore, sees the water interface as a nearly isothermal, nearly rigid boundary; so once the benzene Rayleigh number nears 1708 there is a tendency for buoyancy convection to begin. In the upper fluid, however, buoyancy tends to cause fluid to rise at relatively hot spots and thus draw surface fluid to these spots. The surface tension mechanism, on the other hand, tends to pull the surface and adjacent fluid away from these hot spots. Buoyancy in the water phase also tends to support motion in the direction of the Marangoni-induced surface motion. Two counteractive mechanisms thus compete to control the surface flow, so that motion occurs only after one mechanism dominates the surface flow. Here surface tension gradients are large enough to overcome the counter flow supported by the density gradient, at least for the fluid adjacent to the surface.

A single-cell response in each fluid is expected, as occurs for the Marangoni modes of the system, so that the two-cell response of the benzene at the critical state therefore seems unusual. Two cells certainly result in more viscous dissipation than would occur in a single cell. This fact alone does not preclude a response of this type. The two energy input mechanisms clearly tend to do work at the interface in opposition to each other. Nield's (1964) one-fluid analysis indicates that when the two mechanisms are in opposition, as occurs in these buoyancy modes, the critical Marangoni or Rayleigh number is raised above the maximum

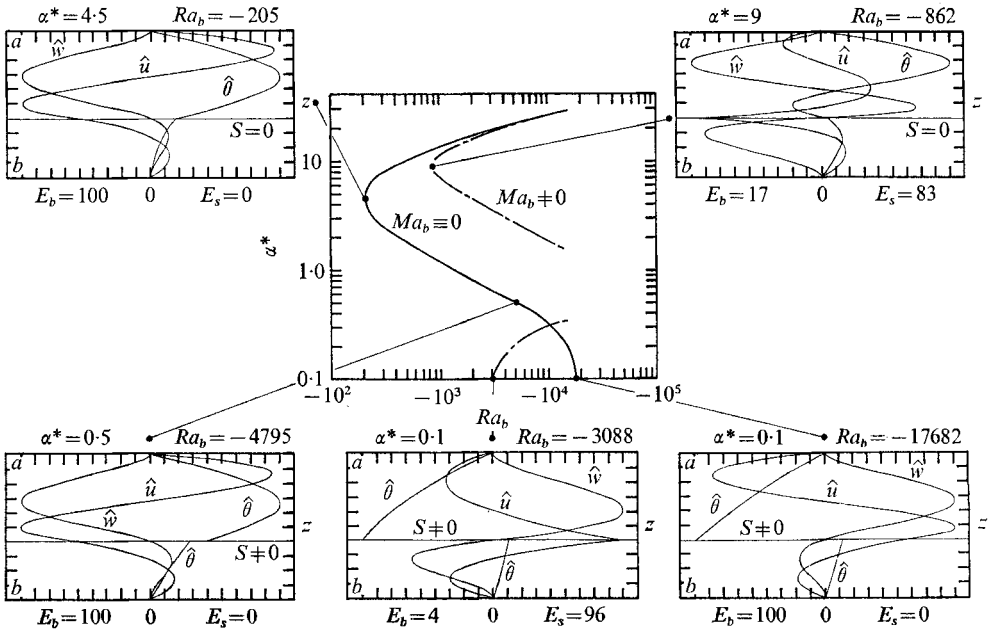

FIGURE 9. Effect of surface tension mechanism on stability for heating from below. Depth fraction = 0·40.

for a single mechanism. He does not present eigenfunctions, however, so the detailed response of this system is not known. In addition, figure 9 shows the Rayleigh number as a function of wavenumber for $d_b^* = 0{\cdot}4$ both with and without the Marangoni effect. The critical Rayleigh number is substantially reduced when surface tension gradients are not allowed. The eigenfunctions for the pure buoyancy flow show that only one cell exists in each phase. Instability also occurs for $\alpha^* \to 0$ for the purely density driven case. The perturbation temperature profiles in both fluids are nearly linear for $\alpha^* = 0{\cdot}1$, again a minimum response to surface tipping.

Single-cell response occurs in both fluids for the surface-tension-gradient driven modes ($d_b^* = 0{\cdot}6 - 0{\cdot}9$). The Rayleigh numbers in both fluids remain well below the critical value for these cases, so the two mechanisms are not in actual conflict. The Marangoni effect must overcome the tendency for the benzene to circulate in the direction opposite to the surface motion, but need not overcome actual motion. Eigenfunctions and energy integrals for other depth fractions are given in I.

4. Comparison with experiment

Initiation of Marangoni convection has been visually observed in flow morphology studies, for example, Berg, Boudart & Acrivos (1966) and Koschmieder (1967). Visible motions presumably have sufficiently large amplitude for nonlinear interactions to be important. Therefore visually determined critical Marangoni numbers can be compared only qualitatively to the predictions of linear stability theory.

Experimental measurements of critical Marangoni number for layers of total depth 2 mm composed of benzene over water were made for heating from above and below as part of the present work. Because of the difficulty of establishing thin layers of benzene over water, experiments were performed only at water depth fractions of 0·40. The initiation of convection was determined by detecting the resulting increase of the heat transfer through the layers above the value for pure conduction. Results for measurable-amplitude motions can be back-extrapolated to determine critical Marangoni number for infinitesimal motions. This is the same technique as that used by Schmidt & Milverton (1935) and Silveston (1958) to determine critical Rayleigh number for fluids confined between horizontal isothermal solid surfaces.

The apparatus is primarily a device for determining the overall thermal conductance of horizontal fluid layers. The test liquids are contained inside a glass cylinder between three-quarter inch thick, twelve inch diameter copper plates spaced by quartz posts. One plate is electrically heated and the other water cooled. Heat transfer through the layers is deduced from an energy balance on the heated plate. Both plates are carefully guard heated or cooled as necessary to minimize energy losses to the environment. Primary plate temperature difference is measured with a four-couple thermopile; additional thermocouples allow monitoring of the plate temperature level and plate-to-guard temperature difference. Each plate assembly is constructed so that either the heated or cooled plate can be the upper or lower face of the test section. The lower plate assembly is supported on jacks for levelling. Sufficient peripheral equipment is provided to stabilize, control and measure input electrical power, to regulate, control and measure energy flux of the cooling water and to monitor all temperatures. The apparatus and the associated data reduction program reproduce the thermal conductivity of water to within 2 % of previously tabulated values and yield a critical Rayleigh number of 1700 ± 150 for a single fluid heated from below. A more detailed description of the apparatus is given in I.

Results for heating from above for two water depth fractions appear in figure 10. No increase in effective thermal conductance of the layers was measurable for Marangoni numbers up to five times the predicted critical value.

The lack of convection may be due to one of two phenomena. The presence of surface contaminants, even in trace amounts, can suppress the Marangoni effect, as has been shown by Berg & Acrivos (1965). Any thermally induced convective motion tends to sweep a contaminant away from the low-surface-tension, warmer regions of the surface. Since surface tension is normally reduced by the presence of foreign substances, the resulting surface concentration profile causes a surface tension gradient which opposes the thermally induced gradient. Surface tension is much more strongly dependent on chemical species concentration than temperature, so that extermely small concentrations of contaminants may nullify the thermally induced Marangoni effect. Berg, Boudart & Acrivos (1966) were unable to detect Marangoni effect evaporative convection in water. They suggest that the large surface tension of water is very easily reduced by contamination, thus shutting off the surface mechanism. Measurements of water–benzene interfacial tension with a ring tensiometer showed no measurable variation for the

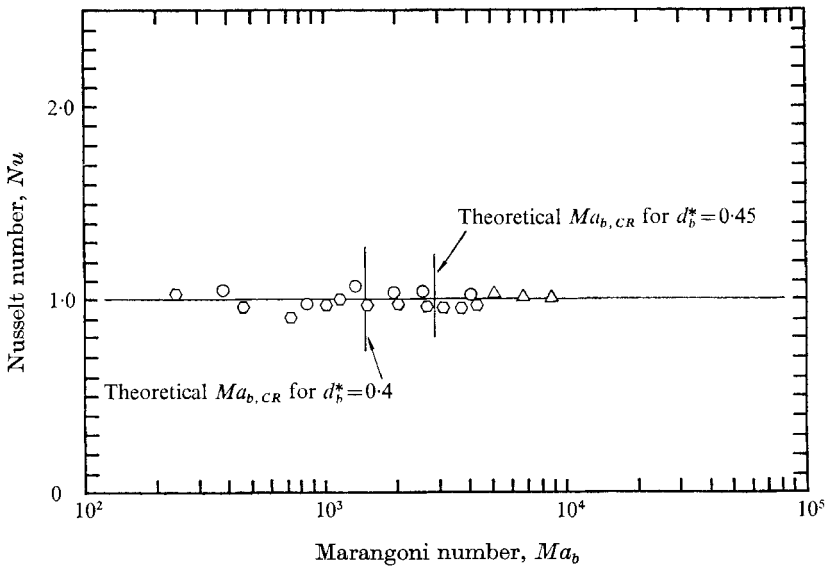

FIGURE 10. Nusselt number versus Marangoni number for heating from above. Benzene over water, total depth 2 mm. Water depth fraction: ⬡, 0·39; △, 0·39; ○, 0·46.

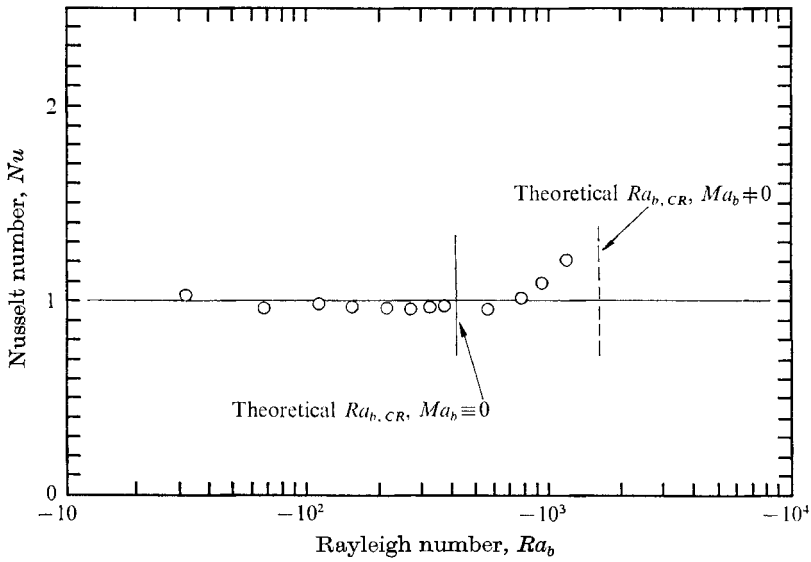

FIGURE 11. Nusselt number versus Rayleigh number for heating from below. Benzene over water, total depth 2 mm, water depth fraction 0·40.

same sample over a period of days. The uncertainty in these measurements is about 5 %, however, and much smaller variations in interfacial tension due to contamination can suppress the thermally driven Marangoni effect. No visible evidence of contamination was noted for these tests, but again, contamination need not be visible for the Marangoni effect to be suppressed. The present analysis does not account for interfacial contamination.

It is also possible that, while this system is unstable for infinitesimal disturbances when heated from above, finite disturbances are damped or amplitude-limited by interactions with the stable density gradient field. That is, no measurable convection actually occurs. A nonlinear analysis would be required for a theoretical examination of this hypothesis.

Results for a water depth fraction of 0·4 for heating from below are shown in Rayleigh number co-ordinates in figure 11. A distinct break in the data occurs, corresponding to a Rayleigh number of 700 or a Marangoni number of about 2800. Values of the critical Rayleigh number with and without the Marangoni effect are also indicated in the figure. The calculations were carried out for properties evaluated at 36 °C, the approximate experimental mean fluid temperature. Property ratios and input parameters at this temperature are collected in table 2.

Figure 9 shows that pure buoyancy driven flow occurs at a critical Rayleigh number less than the critical Rayleigh number for the case when the Marangoni effect is also present. The fact that the measured critical Rayleigh number falls between these limits suggests that surface contamination has retarded, but not completely suppressed, the Marangoni effect in these experiments.

Berg & Morig (1969) studied the effect of density gradient on Marangoni convection caused by acetic acid transfer across a water/benzene + chlorobenzene interface. Varying the chlorobenzene concentration in the benzene resulted in stabilizing or destabilizing density gradients in either or both phases. Stabilizing density gradients confined the Marangoni convection to a region near the interface, with no apparent motion in the bulk fluid. Nearly neutral density gradients resulted in a quasi-cellular flow involving much of the bulk fluid. Unstable density gradients produced motions extending deep into the unstably stratified fluid, with intense small-scale agitation in a thin layer adjacent to the interface.

The results of their experiments are in qualitative agreement with the analysis presented here. The tendency for the motion to be suppressed and confined near the interface for stably stratified fluid is predicted by this analysis as is the greater involvement of fluid for unstable stratification. The intense agitation near the interface suggests the two-cell critical state also found in the analysis.

5. Conclusion

Including density variation in the analysis of two-fluid Marangoni instability significantly alters stability limits. Comparison with Smith's (1966) pure Marangoni effect analysis shows that the critical Marangoni number is increased and certain wavelength disturbances are stabilized when heating is from above. Heating from below lowers the critical Marangoni number and adds a buoyancy driven instability mode. The critical state for the buoyancy mode has two cells in one phase because the two mechanisms tend to drive the interface in opposite directions.

Two classes of flow result, with and without surface deflexion. The critical Marangoni number for some depth fractions occurs for the surface deflected mode, indicating the need to include the possibility of surface deflexions.

Experiments to measure the critical Marangoni number in layers of total depth

2 mm consisting of benzene over water indicate no detectable fluid motion for heating from above. The critical Rayleigh number for heating from below falls between the values predicted with and without the Marangoni effect. Suppression of the Marangoni effect by surface contamination would explain these discrepancies. Qualitative agreement with experiments by Berg & Morig (1969) is shown.

Financial support for this work was supplied by the National Science Foundation. Computer time was donated by Stanford University. The authors would like to acknowledge the helpful comments of the referees.

Appendix. Asymptotic analysis for zero wavenumber

The numerical solutions indicate the existence of a lower branch of the stability loops which appears to have minimum Marangoni number at a wavenumber α^* equal to zero. The values of critical Marangoni number for $\alpha^* = 0$ are found from an asymptotic analysis for $\alpha^* \to 0$. Proceeding by expanding the eigenfunction and the eigenvalue Ma_b (and thus Ra_b) in powers of α^{*2} produces

$$\hat{\theta} = \hat{\theta}^{(0)} + \alpha^{*2}\hat{\theta}^{(1)} + \ldots,$$

$$Ra_b = Ra_b^{(0)} + \alpha^{*2} Ra_b^{(1)} + \ldots,$$

$$Ma_b = Ma_b^{(0)} + \alpha^{*2} Ma_b^{(1)} + \ldots.$$

Substituting into (16) and into the boundary and interface conditions and sorting out powers of α^{*2} yields equations for the different orders of $\hat{\theta}$.

The equations for $\hat{\theta}^{(0)}$ are linear and homogeneous so that a trivial solution is expected. However, linear eigenfunctions corresponding to zero eigenvalues exist for this set. Subsequent solution of the equation set for $\hat{\theta}^{(1)}$ yields, after straightforward manipulation, an expression for Marangoni number at zero wavenumber:

$$Ma_b\left\{\frac{1}{1-k^*} - \frac{\Gamma}{60}\left[11 d_b^{*3} + \frac{\beta^*\rho^*}{k^*} d_a^{*3} + 14\frac{\mu^* d_b^{*4} - (\beta^*\rho^*/k^*) d_a^{*4}}{d_a^{*2} - \mu^* d_b^{*2}}\right]\right\}$$
$$= \frac{2}{3}\frac{1-\rho^*}{1-k^*}\frac{Bo_b}{Cr_b} d_b^*(k^* d_b^* + d_a^*)\left[\frac{\mu^* d_b^*}{d_a^{*2} - \mu d_b^{*2}} + 1\right]. \quad \text{(A 1)}$$

Asymptotic values of Ma_b for various depth fractions of the water–benzene system considered above are indicated in figures 2 and 5 by tick marks below the $\alpha^* = 0{\cdot}1$ axis.

If Γ is set identically zero, (A 1) is valid for the pure Marangoni effect case treated by Smith (1966). Converted to his notation, (A 1) gives values corresponding to the apparent asymptotes in the several cases he presented. The asymptotic limits for the buoyancy-free water–benzene system are indicated by tick marks in figures 3 and 6. Asymptotic values of the Rayleigh number can also be extracted from (A 1).

The critical eigenfunctions corresponding to $\alpha^* = 0$ are the linear temperature profiles consistent with the shifted interface location. There is no accompanying fluid motion.

REFERENCES

BÉNARD, H. 1900 Les tourbillons cellulaires dans une nappe liquid. *Rev. Gen. Sci. Pures Appl. Bull. Assoc. France Avan. Sci.* **11**, 1261, 1309.

BERG, J. C. & ACRIVOS, A. 1965 The effect of surface active-agents on convection cells induced by surface tension. *Chem. Engr. Sci.* **20**, 737.

BERG, J. C., ACRIVOS, A. & BOUDART, M. 1966 Evaporative convection. In *Advances in Chemical Engineering*, vol. 6 (ed. T. B. Drew, J. W. Hoopes & T. Vermeullen), pp. 61–123. Academic.

BERG, J. C., BOUDART, M. & ACRIVOS, A. 1966 Natural convection in pools of evaporating liquids. *J. Fluid Mech.* **24**, 721.

BERG, J. C. & MORIG, C. R. 1969 Density effects in interfacial convection. *Chem. Engrg. Sci.* **24**, 937.

JEFFRIES, H. 1926 The stability of a layer of fluid heated from below. *Phil. Mag.* **2** (7), 833.

JEFFRIES, H. 1928 Some cases of instability in fluid motion. *Proc. Roy. Soc.* A **118**, 195.

KOSCHMIEDER, E. L. 1967 On convection under an air surface. *J. Fluid Mech.* **30**, 9.

LOW, A. R. 1929 On the criterion for stability of a layer of viscous fluid heated from below with an application to meteorology. *Proc. 3rd Int. Congr. Appl. Mech.* **1**, 109.

NIELD, D. A. 1964 Surface tension and buoyancy effects in cellular convection. *J. Fluid Mech.* **19**, 341.

PEARSON, J. R. A. 1958 On convective cells induced by surface tension. *J. Fluid Mech.* **4**, 489.

PELLEW, A. & SOUTHWELL, R. V. 1940 On maintaining convective motions in a fluid heated from below. *Proc. Roy. Soc.* A **176**, 312.

RAYLEIGH, LORD 1916 On convection currents in a horizontal layer of fluid, when the higher temperature is on the underside. *Phil. Mag.* **32** (6), 529.

REID, W. H. & HARRIS, D. L. 1958 Some further results on the Bénard problem. *Phys. Fluids*, **1**, 102.

SCHMIDT, R. J. & MILVERTON, S. W. 1935 On the stability of a fluid when heated from below. *Proc. Roy. Soc.* A **152**, 586.

SCRIVEN, L. E. & STERNLING, C. V. 1964 On cellular convection driven by surface tension gradients: effects of mean surface tension and surface viscosity. *J. Fluid Mech.* **19**, 321.

SILVESTON, P. L. 1958 Warmdurchgang in waagerechten flüssigkeitsschichten. *Forsch. Ing. Wes.* **24**, 29, 59.

SMITH, K. A. 1966 On convective instability induced by surface tension gradients. *J. Fluid Mech.* **24**, 401.

STERNLING, C. V. & SCRIVEN, L. W. 1959 Interfacial turbulence: hydrodynamic instability and the Marangoni effect. *A.I.Ch.E. J.* **5**, 514.

VIDAL, A. & ACRIVOS, A. 1966 Nature of the neutral state in surface tension driven convection. *Phys. Fluids*, **9**, 615.

ZEREN, R. W. & REYNOLDS, W. C. 1970 Thermal instabilities in horizontal two-fluid layers. *Thermosciences Division Rep., Department of Mechanical Engineering, Stanford University*, no. FM-5.